

Surface movement in water of splendipherin, the aquatic male sex pheromone of the tree frog *Litoria splendida*

Adam W. Perriman¹, Margit A. Apponyi², Mark A. Buntine², Rebecca J. Jackway², Mark W. Rutland³, John W. White¹ and John H. Bowie²

¹ Research School of Chemistry, Australian National University, Canberra, Australia

² Department of Chemistry, The University of Adelaide, Australia

³ Department of Chemistry, Royal Institute of Technology, Stockholm, Sweden

Keywords

2D NMR; splendipherin; sex pheromone; surface pressure gradient; X-ray reflectometry

Correspondence

J. H. Bowie, Department of Chemistry, The University of Adelaide, Adelaide, SA 5005, Australia

Fax: +61 8 8303 4358

Tel: +61 8 8303 5767

E-mail: john.bowie@adelaide.edu.au

(Received 4 March 2008, revised 8 April 2008, accepted 29 April 2008)

doi:10.1111/j.1742-4658.2008.06483.x

The aquatic sex pheromone splendipherin (GLVSSIGKALGGLADV-VKSKGQPA-OH) of the male green tree frog *Litoria splendida* moves across the surface of water to reach the female. Surface pressure and X-ray reflectometry measurements confirm that splendipherin is a surface-active molecule, and are consistent with it having an ordered structure, whereby the hydrophilic portion of the peptide interacts with the underlying water and the hydrophobic region is adjacent to the vapour phase. The movement of splendipherin over the surface of water is caused by a surface pressure gradient. In order to better define the structure of splendipherin at the water/air interface we used 2D NMR studies of the pheromone with the solvent system trifluoroethanol/water (1 : 1 v/v). In this solvent system, splendipherin adopts a bent α helix from residues V3 to K21. The bending of the helix occurs in the centre of the peptide in the vicinity of G11 and G12. The region of splendipherin from V3 to G11 has well-defined amphipathicity, whereas the amphipathicity from G12 to A25 is reduced by K19 and P24 intruding into the hydrophobic and hydrophilic regions respectively. A helical structure is consistent with X-ray reflectometry data.

Pheromones are substances that are released to cause a behavioural response in a particular species, and are commonly involved in mating and courtship. Amphibians evolved in the Devonian period from freshwater fish and it might be expected that amphibians would have both terrestrial and aquatic pheromones. It is known that fish have two types of sex pheromones, namely (a) water-soluble pheromones which can attract the male and/or female, however, little is known of the chemistry of these pheromones, and (b) pheromones which are transferred directly to the female by the male when they are close enough to touch, some of these have been identified as steroidal-type molecules [1–7].

The evidence that there are aquatic sex pheromones in fish suggests that amphibians should carry through

(or modify) these pheromones. Because anurans produce many peptides in their glandular secretions [8], water-soluble pheromones may be peptides. Initial support for this proposal came from the report of a peptide pheromone in the mud crab, *Rhithropanopeus harrisi* [9], and the isolation of attractin, a peptide pheromone from a mollusc [10]. Alarm responses were detected in *Bufo bufo* tadpoles as early as 1949 [11], but the first report of an aquatic male sex pheromone from an amphibian appeared in 1995 [12–14]. This was a small peptide, named sodefrin (SIPSKDALLK-OH), isolated from the aquatic Japanese fire-bellied newt *Cynops pyrrhogaster*. A similar peptide, silefrin (SILSKDAQLK-OH), is the male sex pheromone of the related aquatic newt *Cynops ensicauda* [15]. Both sodefrin and silefrin are contained in the cloacal gland of

Abbreviation

HSQC, heteronuclear single-quantum coherence.

the newt. The male releases the pheromone in water, and waves its tail vigorously to distribute the pheromone and attract the female [12–15]. A 22 kDa proteinaceous courtship pheromone has been discovered in a terrestrial salamander, *Plethodon jordani* [16]. This is deposited directly onto the skin of the female during courtship displays on land. The pheromone comes from the mental gland (located under the chin) of the male [16].

The first reported anuran sex pheromone was isolated from the magnificent tree frog *Litoria splendida* [17,18]. Monthly secretions from the parotoid glands were collected from male and female frogs over a period of 3 years using the benign electrical stimulation method [18]. HPLC separation of these secretions indicated a minor component, contained only in male secretions, the level of which peaks during the reproductive period of the frog. This was identified as the male sex pheromone splendipherin, a 25-residue peptide (GLVSSIGKALGGLLADVVKSKGQPA-OH). Behavioural tests carried out in a $2 \times 0.65 \times 0.75$ m glass tank containing a 2 cm depth of (static) water, showed that females were attracted to the splendipherin source at total tank concentrations as low as 10 pM. Females noted the presence of splendipherin within 20 s of the pheromone being placed in cotton gauze at the end of the tank. The peptide does not move towards the female by agitation of the water (as is the case with sodefrin and silefrin) nor is there direct application to the female (as in the case of *P. jordani*). Because recognition of splendipherin by the female occurs some 20 s after the pheromone is pipetted into the cotton gauze, diffusion through static water can be eliminated as a mechanism of transfer due to the time-scale of the diffusion process. It has been proposed that splendipherin moves across the surface of the water by surfactant motion [18].

In this study we: (a) confirmed experimentally that movement of splendipherin occurs on the surface of the water, (b) used X-ray reflectometry and surface-pressure measurements to confirm the surface activity of the pheromone, and (c) used 2D NMR spectroscopy to suggest a possible ordered structure for splendipherin at the air/water interface.

Results

In this section we deal separately with three different types of experiment, bringing these three aspects of the study together in the Discussion. The results of the experimental work outlined below are dealt with serially, namely: (a) behavioural experiments which show that the pheromone splendipherin spreads rapidly

across the surface of static water; (b) the use of surface-pressure measurements and X-ray reflectometry to show that splendipherin is surface active, indicating an ordered peptide structure at the air/water interface; and (c) the use of CD and 2D NMR techniques to suggest that splendipherin may adopt a helical structure at the air/water interface.

Behavioural tests with female *L. splendida*

When a female *L. splendida* was sitting in 2 cm of water in a 2 m glass tank and 40 ng of splendipherin in water was added to a gauze swab anchored to the bottom of the tank 1 m from the female, she recognized the pheromone within 20 s of its placement, walked toward the pheromone source and sat on it. The average time for the frog to reach the pheromone source was 6 min 30 s and the success of these experiments was 100% [18].

Similar experiments have been carried out with a glass partition placed across the tank between the frog and the pheromone source to a depth of 1 cm. Under these conditions, when 40 ng of involatile splendipherin was placed onto the swab, the frog did not recognize the pheromone. When 4 µg of splendipherin was then placed on the swab the female still made no movement towards the pheromone source. These experiments were carried out in the breeding season (February, in the southern hemisphere summer) using two sexually mature female frogs, on six occasions each. This eliminates the possibility of a diffusion mechanism and confirms the previous suggestion [18] that the pheromone must move across the surface of the water.

The surface activity of splendipherin at the air/water interface

In light of the surface movement of the pheromone detailed above, the surface activity of splendipherin was investigated by spreading 30 µL of a $1 \text{ mg} \cdot \text{mL}^{-1}$ solution of the peptide on the surface of water contained in a polytetrafluoroethylene trough. The area of the trough was controlled by a motorized polytetrafluoroethylene barrier, and surface pressure was measured as a function of trough area. Because the amount of peptide introduced to the air/water interface was known (Γ_{applied}), the surface pressure (π) was expressed as a function of the average area per molecule (A). To complement this analysis, X-ray reflectometry measurements were made at various trough areas (Fig. 1). These measurements provide a measure of the volume fraction of the peptide (ϕ_{prot}) perpendicular to the water surface and the surface concentration of the peptide (Γ_{measured}).

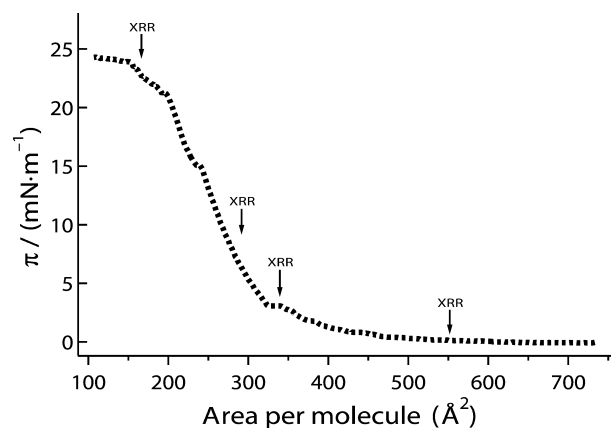


Fig. 1. The pressure–area isotherm after spreading 30 μL of a 1 $\text{mg}\cdot\text{mL}^{-1}$ solution of splendipherin. π is the surface pressure. The arrows show the surface pressures at which reflectivity measurements were taken.

The pressure–area isotherm after spreading splendipherin at the air/water interface is presented in Fig. 1. Upon compression of the layer, little change in surface pressure was observed until an area per molecule of $\sim 550 \text{ \AA}^2$ was reached. This shows that above this area, splendipherin exists in a quasi-2D gas state, in which there are few interactions between the molecules in the layer.

As the layer was compressed further, a steady increase in surface pressure was observed, before reaching a small plateau at $340 \text{ \AA}^2\cdot\text{molecule}^{-1}$. The difference in reflectivity at 550 and $344 \text{ \AA}^2\cdot\text{molecule}^{-1}$ was significant (supplementary Fig. S2; cf. supplementary Figs S1 and S3), i.e. there was an increase in reflectivity after compression, resulting from an increase in the amount of peptide per unit area. Both reflectivity datasets could be fitted using a model describing a single layer of peptide, and yielded peptide layer thicknesses (τ) of 13 (1) \AA (figure in parentheses is the experimental uncertainty based on the standard deviation [52]). Although there was no change in the thickness of the peptide layer upon compression, there was a large increase in the peptide volume fraction (ϕ_{prot}), from 0.45 (0.02) to 0.79 (0.05). This increase in volume fraction is illustrated in Fig. 2, which shows the volume fraction profiles resulting from the reflectivity data fitting.

The increase in volume fraction after compression also resulted in an increase in the surface concentration (Γ_{measured}), which was 0.8 (0.1) $\text{mg}\cdot\text{m}^{-2}$ at $550 \text{ \AA}^2\cdot\text{molecule}^{-1}$, and 1.3 (0.2) $\text{mg}\cdot\text{m}^{-2}$ at $344 \text{ \AA}^2\cdot\text{molecule}^{-1}$. Good agreement between Γ_{applied} and Γ_{measured} at both areas shows complete conservation of material at the air/water interface, signifying a high level of surface

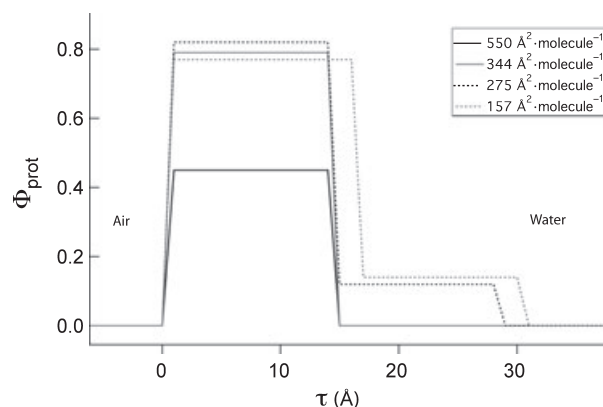


Fig. 2. Volume fraction (ϕ_{prot}) profiles of splendipherin at the air/water interface. τ is the peptide layer thickness. The layer has been compressed to give an area per molecule of 550 \AA^2 (black line), 344 \AA^2 (grey line), 275 \AA^2 (black dashed line) and 157 \AA^2 (black dashed line).

activity. These parameters and all others resulting from the reflectivity data fitting are summarized in Table 1.

Further compression beyond the plateau ($\sim 340 \text{ \AA}^2\cdot\text{molecule}^{-1}$) resulted in a rapid increase in the surface pressure, showing an increase in intermolecular repulsions as the area/molecule was reduced. Effective fitting of the reflectivity data in this region (area/molecule of 275 \AA^2) could be achieved only using a two-layer model, consisting of a dense ($\phi_{\text{prot}} = 0.8$) upper (nearest the air) layer and a diffuse lower ($\phi_{\text{prot}} = 0.12$) layer (towards the solution bulk). The thickness of these layers was 13.3 (0.8) and 13.9 (1.3) \AA , respectively. The resulting volume fraction profile is given in Fig. 2.

At $\sim 15 \text{ mN}\cdot\text{m}^{-1}$ ($250 \text{ \AA}^2\cdot\text{molecule}^{-1}$), a kink is apparent in the pressure/area isotherm of splendipherin (Fig. 1), and at higher pressures three regions of decreasing slope can be seen. To investigate the cause of this behaviour, the area of the trough was held constant and the surface pressure was monitored (data not shown). It was found that surface pressures $> 10 \text{ mN}\cdot\text{m}^{-1}$ ($< 260 \text{ \AA}^2\cdot\text{molecule}^{-1}$) were not stable, but decreased over time. This decrease was more rapid at higher pressures.

Reflectivity was recorded when the film was near the compression maximum ($157 \text{ \AA}^2\cdot\text{molecule}^{-1}$), and the data were fitted using the two-layer model described above. The resulting volume fraction profile is shown in Fig. 2, and deviates only slightly from that of $275 \text{ \AA}^2\cdot\text{molecule}^{-1}$. At $157 \text{ \AA}^2\cdot\text{molecule}^{-1}$, however, the applied surface excess (Γ_{applied}) was much greater than the measured surface excess (Γ_{measured}), which shows that significant desorption has occurred (Table 1). As discussed above, this was not observed at lower pressures, where there was good agreement between Γ_{applied}

Table 1. X-ray reflectivity fitting parameters from 30 μL of 1 $\text{mg}\cdot\text{mL}^{-1}$ splendipherin spread at the air/water interface. Figures in parentheses indicate the experimental uncertainty based on the standard deviation [52].

Area/molecule (\AA^2)	Layer	τ (\AA)	ϕ_{prot}	Γ_{applied} ($\text{mg}\cdot\text{m}^{-2}$)	Γ_{measured} ($\text{mg}\cdot\text{m}^{-2}$)
550 (7)	1	13.2 (1.0)	0.45 (0.02)	0.7 (0.01)	0.8 (0.1)
344 (4)	1	12.8 (0.7)	0.79 (0.06)	1.2 (0.01)	1.3 (0.2)
275 (3)	1	13.3 (0.8)	0.82 (0.06)	1.4 (0.02)	1.6 (0.2)
	2	13.9 (1.3)	0.12 (0.03)		
157 (2)	1	14.8 (0.6)	0.77 (0.04)	2.5 (0.03)	1.8 (0.1)
	2	14.3 (1.3)	0.14 (0.02)		

and Γ_{measured} . From this it is apparent that below a threshold pressure of $\sim 10 \text{ mN}\cdot\text{m}^{-1}$, there is no significant desorption of splendipherin from the surface.

These results confirm that splendipherin is surface active with dimensions consistent with an ordered structure on the surface of water (see Discussion). The CD and 2D NMR experiments outlined below are designed to study that ordered structure.

NMR structural studies

Solvent

The solvent system chosen for a 2D NMR study plays a major role in determining the extent of peptide secondary structure formation. For example, some amphibian skin peptides are unstructured when dissolved in water, but when dissolved in a mixture of water and trifluoroethanol, a solvent that mimics the membrane surface, they are able to fold into the conformation they would adopt in a membrane-surface environment [8]. A mixture of trifluoroethanol and water can be described as a structure-promoting solvent. When there is a tendency for a peptide to form an ordered secondary structure, this solvent system will enhance the formation of such a structure, but it will not cause a secondary structure to form if it is not already inherently programmed into the sequence [19,20]. Although the mechanism by which trifluoroethanol/water enhances structure formation is poorly understood, it continues to be a favoured membrane-mimicking solvent [20,21]. (A reviewer indicated that determining the structure of splendipherin in micelles would give a more accurate picture of the 3D structure. This is certainly true in a general sense. However, we have previously carried out NMR studies of peptides in both of these solvent systems, and found that any differences are in the fine detail, whereas the overall structure is little influenced by measuring the NMR spectra of the peptide in micelles [22,23]. As a consequence we now routinely use the trifluoroethanol/water solvent system for such peptides). The ratio of water to trifluoroethanol used for the NMR study was determined by CD spectroscopy as outlined below.

CD spectroscopy

CD spectra were acquired for splendipherin in increasing concentrations from 0 to 50% (by vol) of trifluoroethanol in water (supplementary Fig. S4). In the absence of trifluoroethanol, splendipherin exhibits a CD spectrum characteristic of an unstructured peptide, i.e. a broad minima was observed at 196–198 nm. On increasing the trifluoroethanol concentration, the spectra showed a predominantly α -helical structure with two minima in the vicinity of 208 and 220 nm. The CD study shows that at 50% trifluoroethanol the spectrum shows greatest ellipticity, indicative of a structure with maximum helicity.

Structural studies in trifluoroethanol/water (1 : 1 v/v)

It seems reasonable that the air/water interface may stabilize the peptide structure like a 1 : 1 trifluoroethanol/water mixture, as this interface has both hydrophobic (air) and hydrophilic (water) regions [24]. NMR spectra were therefore taken in this solvent system.

Assignment of NOESY and TOCSY spectra was achieved using standard methodology [25]. Because of the trend of chemical shifts towards random-coil values in the centre of the peptide, the N_i – N_{i+1} cross-peaks in the NOESY spectrum of a number of adjacent residues overlapped. In these cases, the α_i – N_{i+n} , β_i – N_{i+1} and α_i – β_{i+3} cross-peaks were used to assign residues in sequence. The resultant chemical shift data are available in Table S1. The assigned HN–NH region of the NOESY spectrum is illustrated in supplementary Fig. S5.

A NOE intensity diagram for splendipherin was constructed and is shown in Fig. 3. It indicates that the majority of the peptide is α -helical, however, there are some peaks that are typically present in an α helix missing towards the C-terminus, indicating a less rigid structure. The increased strength of $d_{\alpha\text{N}(i,i+1)}$ interactions suggests that this region may have an extended conformation.

Of particular importance is the observation that $d_{\text{NN}(i,i+3)}$ peaks are missing in the central G11–G12



Fig. 3. NOE intensity diagram for splendipherin. The thickness of the bands indicates the relative strength of the signal (strong, $< 3.1 \text{ \AA}$; medium, $3.1\text{--}3.7 \text{ \AA}$; weak, $> 3.7 \text{ \AA}$). Grey shaded boxes indicate ambiguous NOEs. Peaks overlapped on the diagonal have been omitted.

region; this indicates some bending/distortion of the α -helical structure in this region. However, this region cannot be regarded formally as a hinge, because the $\alpha, \beta_{i,i+3}$ and $\alpha, N_{i,i+3}$ NOE data in Fig. 3 show that G11 and G12 are not fully flexible.

The predominance of a helical structure for splendipherin was also indicated from an examination of the deviation from random-coil chemical shift values [25–27] of the ^1H and ^{13}C α -CH resonances. Although a complete set of random-coil chemical shifts are not available for the amino acids in trifluoroethanol, those which have been tabulated [28] indicate that there is little difference between random-coil chemical shifts in trifluoroethanol and water. Accordingly, for splendipherin in trifluoroethanol, a comparison was made with random-coil chemical shifts determined in water [26,27]. The chemical shift differences between observed resonances and the random-coil values, $\Delta\delta$, were smoothed over a window of $n \pm 2$ residues and plotted against the amino acid sequence for αH and αC resonances (supplementary Figs S6 and S7).

The α -protons in splendipherin are shifted upfield in the region L14–K19 and to a lesser extent in the region S5–K8. [A reviewer has suggested that the small upfield shifts of the α -protons of S5–K8 (maximum shift, -0.16 ; see supplementary Fig. S6) appear to be at variance with the corresponding α - ^{13}C shifts shown in supplementary Fig. S7 and with NOE data indicating that the region is α -helical. The reason for these small shifts is not obvious, but similar data were obtained in a 2D NMR study of the helical-hinge-helical peptide caerin 1.1 (GLLSVLGSAKHVLPVVPVIAEHL-NH₂), in which the maximum α -proton shift for V5–S8, situated in the first helical region (L2–K11), is -0.21 [29].] This suggests that there are two defined α -helical regions [29]. The shifts from K21

onwards are slightly positive, indicating an extended conformation (supplementary Fig. S6). The secondary shift plot for α -carbon resonances supports this trend. Downfield shifts occur in regions S5–A9 and A15–K19, with residues from K21 onwards showing no helical trend (supplementary Fig. S7).

The HN ^1H secondary shifts of splendipherin in trifluoroethanol/water (1 : 1 v/v) are shown in Fig. 4. The magnitude of the HN secondary shifts deviates periodically over three to four residues, characteristic of an amphipathic α helix due to the differences in hydrogen-bond lengths on either face of the molecule [30]. This trend drops off after residue 21, confirming that the C-terminal end of splendipherin is not α -helical (Fig. 4).

NOE intensities were used as input for the structure calculations, the structure obtained agrees with the conclusions gained from initial inspection of the NMR data. A total of 284 non-redundant restraints were produced for splendipherin of which 56 were sequen-

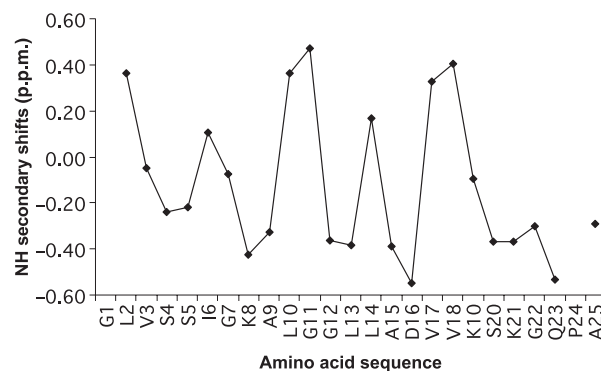


Fig. 4. HN ^1H secondary shifts of splendipherin in trifluoroethanol/water (1 : 1 v/v). Negative values indicate an upfield shift from random coil resonances, whereas positive values indicate a shift downfield.

tial ($i, i+1$), 40 were medium range (two to four residues apart) and 65 were ambiguous. Ambiguous assignments [31,32] were countered by use of the sum averaging method as previously described [33,34]. The restraints are summarized in Table 2.

Analysis of the psi and phi angles of the 20 lowest energy structures shows that there are two well-defined regions, from V3 to L10 and from G12 to K21. The first and last four residues were not expected to be well structured, as the terminal residues in any peptide are less able to form rigid secondary structure because they lack the appropriate hydrogen-bonding network [30], and because the entropy of the disordered state may outweigh the enthalpic advantage of secondary structure formation in this region. Analysis of the ensemble energies of 20 lowest energy structures and of the averaged structure of splendipherin was also performed. The data from this analysis are shown in Table 2, where $\langle SA \rangle$ is the ensemble of 20 lowest energy structures and $(SA)_r$ is the energy minimized averaged structure. Only three violations were present

Table 2. Experimental restraints, X-PLOR energies and violation statistics and rmsd data for the splendipherin structures.

Type of restraint	Number of restraints	Percentage
Sequential	56	19.72
Medium-range	40	14.08
Long-range	0	0
Intraresidue	123	43.31
Ambiguous	65	22.89
Total	284	100
<hr/>		
X-PLOR energies (kcal·mol ⁻¹)	$\langle SA \rangle$	$(SA)_r$
E_{tot}	56.48	36.32
E_{bond}	3.99	2.16
E_{angle}	21.09	15.96
E_{improper}	3.29	1.64
E_{vdw}	4.42	2.48
E_{NOE}	23.67	14.08
E_{cdih}	0	0
<hr/>		
Violations		
No. of NOES violated > 0.3	3	0
Maximum violation	0.4 Å	0
<hr/>		
rmsd from mean geometry (Å)		
Region	Backbone atoms	Heavy atoms
Entire backbone	2.40 ± 0.87	2.72 ± 0.76
Residues 3–21	1.18 ± 0.51	1.62 ± 0.49
Residues 3–10	0.36 ± 0.11	0.91 ± 0.27
Residues 12–21	0.23 ± 0.06	0.91 ± 0.10

in the ensemble, which indicates that the structures fit the NMR data very well. The maximum violation from the ensemble was 0.4 Å.

Fitting the structures over residues 3–10 and 12–21 shows that each region forms an α helix and that the 20 structures agree well with each other over these stretches (Fig. 5A,B). By contrast, fitting over the length of the peptide, including residue 11, gives significantly less agreement because of some distortion in the centre of the molecule (Fig. 5C). The overlaid structures were generated using the MOLMOL program [35].

Analysis of the angular order parameters (S, psi and phi) of the final ensemble of 20 structures indicated that 18 of the 25 residues (72%) were well defined

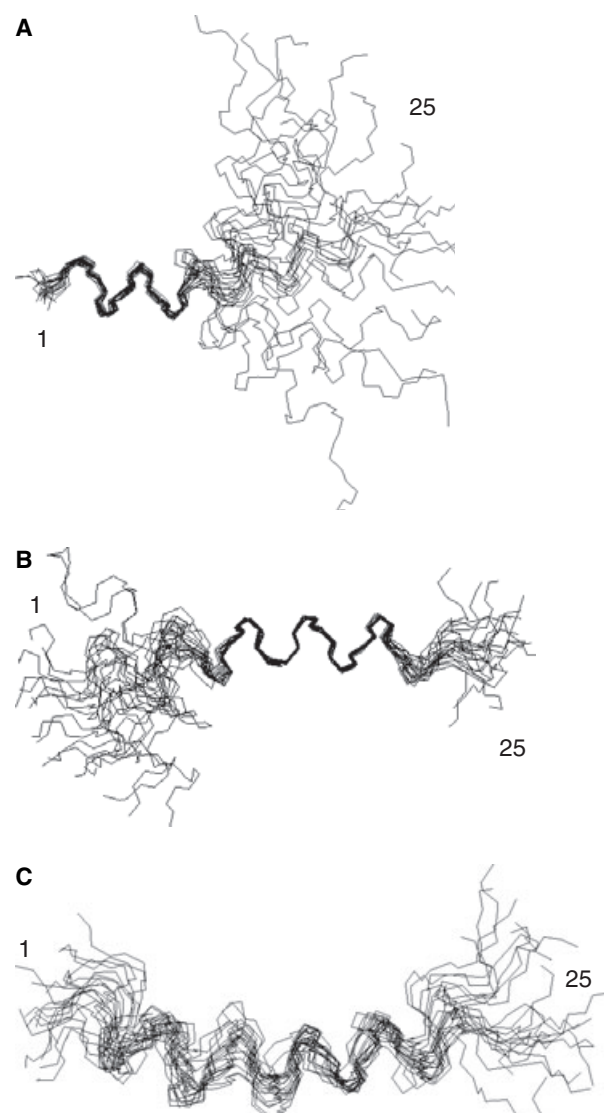


Fig. 5. Low-energy ensemble fitted over (A) residues 3–10, (B) residues 12–21 and (C) the entire well-defined region.

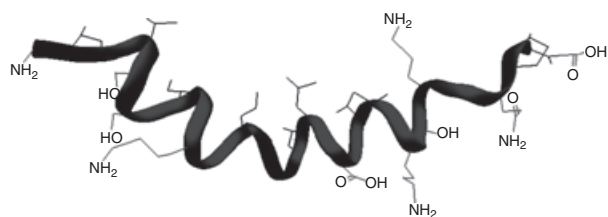


Fig. 6. Lowest energy solution structure of splendipherin.

($S > 0.9$ for psi and phi). This corresponds to regions 3–10 and 12–21, indicating that there is some bending/distortion of the central G11–G12 region. A Ramachandran plot [36] for average psi and phi angles of the peptide showed that all well-defined residues were distributed within the favoured or allowed regions for an α -helical structure, except for Q23. This residue is bordered by a glycine and a proline, both helix-breaking residues, and this region is not helical in nature (data not shown). The rmsd data are listed in Table 2, and show low values for residues within the two helical regions.

The computed lowest energy solution structure is shown in Fig. 6. This illustrates the bent helical structure from V3 to K21 and that the bending is mainly around G11 and G12.

Discussion

Behavioural tests show that when a surface barrier is placed in the tank between the frog and the pheromone source, the animal does not respond to splendipherin. This proves that the movement of splendipherin is not due to bulk diffusion [37]. When the surface barrier is removed, the female frog detects the pheromone 20 s after 40 ng splendipherin (dissolved in 100 μ L of water) is pipetted into a cotton swab anchored to the bottom of the tank. Because the frog is initially 1 m from the pheromone source, the minimum average spreading velocity of splendipherin on the surface of water is 5 cm s^{-1} .

Splendipherin is the first reported example of an aquatic pheromone which can move across the surface of water rather than through it.

The high level of surface activity displayed by splendipherin is illustrated by the complete conservation of material introduced to the air/water interface, and by the high volume fraction of adsorbed peptide (~ 0.8 ; Results, Table 1). This high affinity for the air/water interface is not shared by all peptides, as demonstrated for the designer peptide Lac21E, which at neutral pH, adsorbs with a maximum volume fraction of only 0.17 [38].

This surface activity results from the spatial hydrophobic distribution of the amino acid side chains in a peptide [39]; hydrophilic residues interact with the water phase, whereas the hydrophobic side chains are situated away from the surface towards the air phase. This is indicative of an ordered peptide structure at the water/air interface. Such a distribution has been shown for the surface-active fragment of myoglobin (peptides 1–55), which adsorbs with the helical axes in the plane of the air/water interface [40]. Similar behaviour has been noted for the two synthetic peptides A-peptide and His-peptide [41]. Here the authors used a helix-inducing solvent in conjunction with CD to test the propensity of the peptides to adopt helical conformations. The peptides were then studied at the air/water interface using FTIR reflection absorption spectroscopy and surface-pressure measurements, which showed the peptide helices orientated parallel to the air/water interface. Recent studies using the designer peptide surfactant AM1 (and deuterated analogues) have also shown adsorption with helices orientated parallel to the air/water interface [38,42–44]. Here the peptide is shown to be a random coil (in water) and converts to a helical structure upon adsorption at the air/water interface.

X-ray reflectometry data and surface pressure measurements indicate an ordered structure for splendipherin at the water/air interface. Can we provide data to support the formation of such a structure for splendipherin? If adsorption at the air/water interface stabilizes the secondary structure of peptides of this type, then we could utilize a structure-forming solvent for this purpose. We used 2D NMR spectroscopy in the solvent system trifluoroethanol/water (1 : 1 v/v) to model the interfacial structure.

The lowest energy structure of splendipherin determined by 2D NMR spectroscopy in trifluoroethanol/water (1 : 1 v/v) is shown in Fig. 6. This is used as a model for the structure of splendipherin at the water/air interface. The arrangement of the hydrophobic and hydrophilic regions of the peptide is shown in Fig. 7. Figure 7A shows a spatial hydropathic distribution indicative of surface-active biological molecules, with the hydrophobic and hydrophilic regions on opposite sides of the helix. Figure 7B displays a more random hydropathic distribution with respect to the helical axis (the C-terminal amphipathicity is reduced by K19 and P24 intruding into hydrophobic and hydrophilic regions respectively), and would thus be expected to be less surface active than the N-terminal region of the peptide. At areas per molecule of 550 and 344 \AA^2 , however, a single film thickness of 13 \AA was observed. This is close to the cross-sectional dia-

meter of an α helix (~ 12 Å), indicating a preferential parallel orientation for the helices at the air/water interface, suggesting little or no bending of the second fragment in the direction of the solution bulk.

When the monolayer was compressed to give a molecular area of 275 Å², the formation of a second, more diffuse layer was observed (Table 1). When adopting a linear conformation, the limiting area of the peptide is ~ 420 Å². The formation of the second layer upon compression can be explained by some bending of the peptide in the subphase direction in the vicinity of G11 and G12. Using the layer thicknesses and the dimensions of the two fragments the central angle can be estimated at $> 30^\circ$ from the horizontal surface plane, consistent with the structure shown in

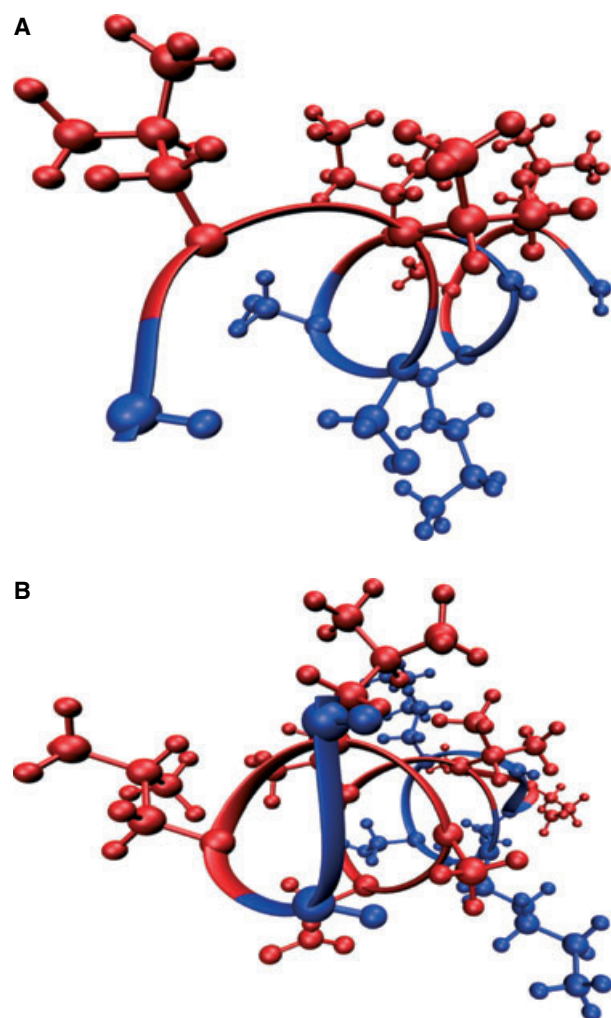


Fig. 7. NMR solution structure of splendipherin as two fragments (**a** = G1–G11 and **b** = G11–A25). The hydrophobic residues are red and the hydrophilic residues blue. The models were generated using visual molecular dynamics and are displayed in perspective view [45].

Fig. 6. Thus the X-ray reflectometry data can be interpreted in terms of an essentially helical structure for splendipherin, as shown in Fig. 6.

Behavioural tests show that the minimum average spreading velocity of splendipherin on the surface of water is 5 cm·s⁻¹. It is not possible to calculate precisely the concentration of the spreading pheromone on the surface (because the rate will decrease as radial spreading increases), but a qualitative estimate can be made at the surface above the swab. The initial drift speed of splendipherin from the top of the swab into the water is estimated at 1.2 cm·s⁻¹ (see Experimental procedures). This drift speed decreases as the splendipherin moves away from the swab; it is estimated that splendipherin takes 1.4 s to travel 1 cm vertically from the swab to the water surface (see Supplementary material). If there is 5 ng of splendipherin in an area of 1 cm² on the surface of the water directly above the swab, the area per molecule in that 1 cm² area is 7900 Å² (see Experimental procedures). As the pheromone molecules on the surface move away from the source, the surface area per molecule of splendipherin increases. X-Ray reflectometry data indicate that once the area per molecule is ≥ 550 Å², there is little interaction between splendipherin molecules and no tendency for the molecule to leave the surface by desorption. The difference in surface tension between the pure water surface and that containing splendipherin decreases with molecular area [44–46], but there will always be some surface pressure gradient, even when the pheromone concentration on the surface is small. Such a system is called a gaseous monolayer [47], and the process can be classified within those phenomena known as Gibbs–Marangoni effects [48–50]. It is the surface pressure gradient that is responsible for the movement of splendipherin across the surface of water.

Conclusions

X-Ray reflectometry surface measurements with splendipherin demonstrate that the peptide is surface active, adopting an ordered structure at the water/air interface. The structure of splendipherin, as determined by 2D NMR studies in trifluoroethanol/water (1 : 1), is proposed as a model for the structure of this pheromone on the surface of water. The structure is essentially α -helical between V3 and K21 with some bending in the centre of the peptide in the vicinity of G11 and G12. Splendipherin moves across the surface of water as a consequence of a surface pressure gradient. This is a unique finding, the first example of an aquatic peptide pheromone which moves across the surface of water by a surface pressure gradient.

Experimental procedures

Synthesis of splendipherin

Splendipherin of > 95% purity was synthesized by Mimotopes (Victoria, Australia) using L-amino acids by the standard N- α -Fmoc method. Full details including protecting groups, and deprotection have been reported previously [51].

Behavioural testing with splendipherin

This work conforms with the Code of Practice for the Care and Use of Animals for Scientific Purposes (1990) and the Prevention of Cruelty to Animals Act (1985), and was approved by The University of Adelaide Animal Ethics Committee.

A female *L. splendida* was allowed to sit for 5 min in the centre of a 2 m aquarium containing water to a depth of 2 cm, such that the head of the animal was above water. At either end of the tank were placed submerged cotton swabs into one of which the pheromone was injected. The tank had a removable glass partition situated halfway between the frog and the pheromone source. The partition penetrated 1 cm into the water in order to stop movement of the pheromone on the surface of the water.

With the partition removed, addition of 40 ng of splendipherin in water to a gauze pad 1 m from the frog, elicited a distinct change in posture and an increased degree of alertness in the animal within 20 s of the introduction of pheromone. The female walked through the shallow water towards the pad containing the pheromone, sat on the pad, and remained seated until removed [17,18].

Experiments were then carried out with the partition in place, in which first 40 ng and then 4 μ g of splendipherin in water was added to the cotton swab. These experiments were repeated with two different females, a total of six times. No pheromone activity was noted.

Surface experiments

Surface films were produced by spreading 30 μ L of a 1 mg·mL⁻¹ (0.42 mM) solution of splendipherin in 50% ethanol/water (v/v) on the surface of Milli-Q[®] water (pH 6.5). Spreading was achieved by forming a drop (\sim 5 μ L) of the peptide solution on the tip of a Hamilton syringe, and then touching the water surface until 30 μ L had been delivered. A fully automated Langmuir trough (Nima 601) was used to generate pressure-area isotherms. The trough consisted of a polytetrafluoroethylene barrier which controls the area of the trough and hence the applied surface concentration of the peptide (Γ_{applied} , mg·m⁻²), and a Wilhelmy plate attached to a microbalance to measure the surface pressure. A compression rate of 40 cm²·min⁻¹ was used for all experiments. The temperature of the trough was maintained at 25 °C by water circulation from a thermostat-controlled bath.

The X-ray reflectivities of the films were measured at a number of trough areas using the angle-dispersive instrument at the rotating anode source of the Research School of Chemistry, Australia National University [52]. The CuK α radiation was selected using a graphite (002) monochromator. Alignment of the instrument was achieved by measuring the reflectivity of Milli-Q[®] water and comparing the model parameters with known values [53]. Measurements were made at angles of incidence in the range 0.0–3.4° (0.00–0.48 Å⁻¹) and all data were scaled using the critical edge of a given sample.

Reflectivity measurements were modelled using CXMULF [52], a program incorporating the optical transfer matrix method of classical optics [54]. The procedure involves calculating the reflectivity, $R(Q_z)$, as a function of the scattering vector, Q_z , using τ , the film thickness (Å), Nb_x , the X-ray scattering length density (Å⁻²), and σ , the Gaussian interfacial roughness (Å) of a series of homogeneous slabs (layers). The calculated reflectivity is then compared with the measured one and the structural parameters modified in a least-squares iteration. All data-sets were first modelled using a single slab, and a second slab was introduced only where necessary. An example of fitting where a double layer model is required is provided in supplementary Fig. S3. This method for fitting reflectometry data from proteins adsorbed at the air/water interface has been shown to be effective [55–57].

To allow evaluation of the volume fraction of peptide, the total volume of the peptide was estimated using amino acid residue volumes [53,58]. Subsequently, the X-ray scattering length density of the pure protein, Nb_{x_prot} , was calculated using:

$$Nb_{x_prot} = \frac{\sum Z_{prot} r_0 N_A \rho_{prot}}{M_w} \quad (1)$$

where $\sum Z_{prot}$ is the number of electrons in a peptide molecule, r_0 is the classical electron radius (2.8×10^{-5} Å), and ρ_{prot} is the physical density of pure peptide. Once the theoretical scattering length density of the pure peptide was evaluated, Eqn (2) was used to evaluate of the volume fraction of protein normal to the surface plane (ϕ_{prot}) [53,55].

$$\phi_{prot} = \frac{Nb_{x_sub} - Nb_x}{Nb_{x_sub} - Nb_{x_prot}} \quad (2)$$

where Nb_{x_sub} and Nb_x are the subphase and measured layer X-ray scattering length densities respectively. The surface excess (Γ , mg·m⁻²) can then be evaluated using Eqn (3):

$$\Gamma = \tau \phi \rho_{prot} \quad (3)$$

where τ is the film thickness.

CD spectroscopy

CD spectra were collected on a Jobin-Yvon CD-6 spectrophotometer at 22 °C. CD spectra were collected at a peptide concentration of 0.4 mg·mL⁻¹, pH 4.7 in H₂O and concentrations of trifluoroethanol from 0 to 50% (v/v) using a method outlined in full earlier [29]. A blank consisting of the appropriate water/trifluoroethanol ratio was run for each sample. Each spectrum represents an average of five scans each with a 2 s integration time, and 1 nm spacing over a wavelength range of 190–240 nm. A pathlength of 0.5 mm was used. Spectra were smoothed using a level 2 smoothing binomial algorithm.

NMR spectroscopy

The solution of splendipherin was prepared by dissolving the unlabelled peptide (6.1 mg) in *d*₃-trifluoroethanol (0.35 mL) and water (0.35 mL), giving a final concentration of 3.4 mM at a measured pH of 2.11. A Varian Inova-600 NMR spectrometer was used for acquisition of all NMR spectra, with a ¹H frequency of 600 MHz and a ¹³C frequency of 150 MHz. Experiments were carried out at 25 °C, and referenced to the methylene protons of residual unlabelled trifluoroethanol (3.918 p.p.m). Referencing of the ¹³C dimension of the heteronuclear single-quantum coherence (HSQC) spectrum was achieved using the ¹³CH₂ signal of trifluoroethanol (60.975 p.p.m). Presaturation allowed for suppression of the water or residual trifluoroethanol hydroxyl resonance in the TOCSY and NOESY experiments and was achieved by centring the transmitter frequency on this resonance and applying low power presaturation from the proton transmitter during a 1.5 s relaxation delay between scans. Gradient methods for suppression were used in the DQF-COSY experiment [57]. TOCSY, DQF-COSY and NOESY experiments were collected in phase-sensitive mode, using time-proportional phase incrementation in *t*₁ [31,59,60]. Typically, 32 time-averaged scans were acquired per increment, with a total of 256 increments for each experiment. The FID in *t*₂ consisted of 2048 data points over a spectral width of 6999.7 Hz, and NOESY spectra were acquired with a mixing time of 150 ms. The HSQC experiment was recorded with an interpulse delay of $1/2J_{\text{CH}} = 3.6$ ms, corresponding to $J_{\text{CH}} = 140$ Hz. Again 256 increments, each comprising 32 scans, were acquired over 4096 data points in the directly detected ¹H, *F*₂ dimension. A spectral width of 24 132.7 Hz was used in the ¹³C, *F*₁ dimension.

A Sun Microsystems Ultra Sparc 1/170 workstation and VNMR software (v. 6.1A) were used to process the resulting spectra. Data matrices were multiplied using a Gaussian function in both dimensions before zero-filling to 4096 data points prior to Fourier transformation. Final processed 2D NMR matrices consisted of 4096 × 4096 real points.

Structure calculations

SPARKY software (v. 3.106) was used to assign ¹H resonances in the NOESY spectra via the sequential assignment procedure [25]. For each symmetric pair of cross-peaks, the volume of the smaller peak was quantified and converted to distance restraints using the method described by Xu *et al.* [61]. ³*J*_{NHCαCH} values were measured from a 1D ¹H NMR spectrum acquired with 0.047 Hz per point digital resolution. Dihedral angles were restrained as follows: ³*J*_{NHCαCH} < 5 Hz, $\phi = -60 \pm 30^\circ$; 5 Hz < ³*J*_{NHCαCH} < 6 Hz, $\phi = -60 \pm 40^\circ$; for ³*J*_{NHCαCH} values ≥ 6, ϕ angles were not restrained.

Structures were generated using X-PLOR software (v. 3.851) and a Sun Microsystems Sparc 1/170 workstation. The restrained molecular dynamics and simulated annealing protocol was used [61], including the use of floating stereo-specific assignments [62]. Ambiguous restraints were managed by sum averaging and refined based on structures resulting from preliminary calculations [34]. Calculations were carried out using the all hydrogen distance geometry force field (v. 4.03) [63]. Sixty structures were generated initially with random backbone torsion angles and subjected to 6500 steps (19.5 ps) of high temperature dynamics at 2000 K. The *K*_{noe} and *K*_{repel} force constants were increased from 1000 to 5000 kcal·mol⁻¹·nm⁻² and 200 to 1000 kcal·mol⁻¹·nm⁻⁴ respectively. Cooling to 1000 K followed in 2500 steps (7.5 ps), with *K*_{repel} increasing further to 40 000 kcal·mol⁻¹·nm⁻⁴, and the atomic radii decreasing from 0.9 to 0.75 times those in the all-hydrogen distance geometry parameter set. Final cooling from 1000 to 100 K then occurred in 1000 steps (3 ps) and resulting structures were subjected to 200 steps of conjugate gradient energy minimization. The 20 lowest potential energy structures produced were selected for analysis. Three-dimensional structures were viewed using INSIGHT II software (v. 95.0, MSI) and the program MOLMOL [35].

Splendipherin molecular area estimation

Assuming 5 ng of splendipherin (molecular mass 2364 Da) in an area of 1 cm² on the surface of the water, the splendipherin surface density is 1.3×10^{12} molecules·cm⁻², or 1.3×10^{-4} molecules·Å⁻². Hence, assuming a uniformly thin surface coverage, an upper bound estimation for the surface area of one splendipherin molecule is ~ 7900 Å².

Splendipherin drift speed estimation

The initial drift speed, *s*₀, of splendipherin from the surface of the swab can be approximated by:

$$s_{\text{zero}} = \frac{-D}{c} \left(\frac{dc}{dx} \right)_0$$

where D is the splendipherin diffusion constant ($\sim 10^{-6} \text{ cm}^2 \text{ s}^{-1}$), c is the initial concentration of splendipherin on the swab and $(dc/dx)_0$ is the initial splendipherin concentration gradient at the surface of the swab.

For a concentration of 40 ng of splendipherin per 100 μL of water deposited on the swab, $c = 1.69 \times 10^{-7} \text{ M}$, and the initial drift speed is therefore:

$$s_0 = -5.9 \frac{dc}{dx} \quad (\text{cm}^2 \text{ s}^{-1} \text{ M}^{-1}).$$

The initial concentration gradient, dc/dx , can be estimated by assuming that the concentration of splendipherin on the swab is $1.7 \times 10^{-7} \text{ M}$ and 0 M in water. Further, assuming a molecular 'length' of splendipherin of $\sqrt{7900 \text{ \AA}^2} = 89 \text{ \AA}$, then $dc/dx \sim -0.2 \text{ M} \cdot \text{cm}^{-1}$. As such, the initial drift speed of splendipherin away from the surface of the swab, $s_0 \sim 1.2 \text{ cm} \cdot \text{s}^{-1}$.

The splendipherin drift speed will decrease as the initial concentration gradient decreases. Assuming that the splendipherin drift speed decreases exponentially as the splendipherin moves through the water away from the swab, the drift speed at the water surface (located 1 cm above the surface of the swab) is $\sim 0.4 \text{ cm} \cdot \text{s}^{-1}$. As such, we estimate that it will take $\sim 1.4 \text{ s}$ for the peptide to reach the water surface, from whence the surface-active motion will commence.

Acknowledgements

We thank the Australian Research Council and the Australian Institute for Nuclear Science and Engineering for financial support of this project. AWP acknowledges the award of an AINSE PhD scholarship. MAA and RJJ acknowledge awards of APA PhD scholarships. The authors wish to thank Dr Duncan McGillivray for useful discussions.

References

- Dulka JG (1993) Sex pheromone systems in goldfish. *Brain Behav Evol* **42**, 265–280.
- Kitamura S, Ogata H & Takashima F (1994) Activities of F-type prostaglandins as releaser sex pheromones in cobite loach *Misgurnus anguillicaudatus*. *Comp Biochem Physiol A Comp Physiol* **107**, 161–169.
- Bjerselius R, Olsen KH & Zheng WH (1995) Behavioural and endocrinological responses of mature male goldfish to the sex pheromone 17- α ,20- β -dihydroxy-4-pregnen-3-one in the water. *J Exp Biol* **198**, 747–754.
- Kime DE & Ebrahimi M (1997) Synthesis of 17,20- α - and 17,20- β -dihydroxy-4-pregnen-3-ones and 11-ketotestosterone and their conjugates by the gills of teleost fish. *Fish Physiol Biochem* **171**, 117–121.
- Zheng WB, Strobeck C & Stacey N (1997) The steroid pheromone 4-pregnen-17- α ,20- β -diol-3-one increases fertility and paternity in goldfish. *J Exp Biol* **200**, 2833–2840.
- Kobayashi MN (1999) 11-Ketotestosterone induces male-type sexual behaviour and gonadotropin secretion in gynogenetic crucian carp, *Carassius auratus langsdorfii*. *Gen Comp Endocrinol* **115**, 178–187.
- Poling KR, Fraser EJ & Sorensen PW (2001) The three steroidal components of the goldfish preovulatory pheromone signal evoke different behaviour in mates. *Comp Biochem Physiol B Biochem Mol Biol* **129**, 645–651.
- Apponyi MA, Pukala TL, Brinkworth CS, Maselli VM, Bowie JH, Tyler MJ, Booker GW, Wallace JC, Carver JA, Separovic F *et al.* (2004) Host-defence peptides of Australian anurans: structure, mechanism of actions and evolutionary significance. *Peptides* **25**, 1035–1054.
- Pettis RJ, Erickson BW, Forward RB & Rittschof D (1993) Superpotent synthetic tripeptide mimics of the mud-crab pumping pheromone. *Int J Peptide Protein Res* **42**, 312–319.
- Painer SD, Clough B, Akal DBG & Nagle GT (1999) Attractin, a water borne peptide pheromone in *Aplysia*. *Invert Reprod Devel* **36**, 191–194.
- Birch MC (1974) *Pheromones*, Vol. **32**. North-Holland, Amsterdam.
- Kikuyama S, Toyoda F, Ohmiya Y, Matsuda K, Tanaka S & Hayashi H (1995) Sodefrin: a female-attracting peptide pheromone in newt cloacal glands. *Science* **267**, 1643–1645.
- Kikuyama S, Yamamoto K, Iwata T & Toyoda F (2002) Peptide and protein pheromones in amphibians. *Comp Biochem Physiol B Biochem Mol Biol* **132**, 69–74.
- Hayashi H & Kikuyama S (1999) Molecular cloning of newt sex pheromone precursor cDNAs: evidence for the existence of species specific forms of pheromones. *FEBS Lett* **457**, 400–404.
- Yamamoto K, Kawai Y, Hayashi T, Ohe Y, Hayashi H, Toyoda F, Kawahara G, Itawa T & Kikuyama S (2000) Silefrin, a sodefrin-like pheromone in the abdominal gland of the sword-tailed newt, *Cynops ensicauda*. *FEBS Lett* **472**, 267–270.
- Rollman SM, Houck LD & Feldhoff RC (1999) Proteinaceous pheromone affecting female receptivity in a terrestrial salamander. *Science* **285**, 1907–1909.
- Wabnitz PA, Bowie JH, Tyler MJ, Wallace JC & Smith BP (1999) Aquatic sex pheromone from a male tree frog. *Nature* **401**, 444–445.
- Wabnitz PA, Bowie JH, Tyler MJ, Wallace JC & Smith BP (2000) Differences in the skin peptides in male and female Australian tree frog *Litoria splendida*. *Eur J Biochem* **267**, 269–275.
- Jasanoff A & Fersht AR (1994) Quantitative-determination of helical propensities from trifluoroethanol titration curves. *Biochemistry* **33**, 2129–2135.

- 20 Sonnichsen FD, Vaneyk JE, Hodges RS & Sykes BD (1992) Effect of trifluoroethanol on protein secondary structure – an NMR and CD study using a synthetic actin peptide. *Biochemistry* **31**, 8790–8798.
- 21 Fan F & Mayo KH (1995) Effect of pH on the conformation and backbone dynamics of a 27-residue peptide in trifluoroethanol – an NMR and CD study. *J Biol Chem* **270**, 24693–24701.
- 22 Chia BCS, Bowie JH, Carver JA & Mulhern TD (2000) The solution and micelle-bound structures of maculatin 1.1, an antibacterial peptides from *Litoria genimaculata*. *Eur J Biochem* **267**, 1894–1906.
- 23 Wegener KL, Carver JA & Bowie JH (2003) The solution and micelle structures of caerin 1.1 and 1.4 in aqueous TFE and dodecylphosphocholine micelles. *Biopolymers* **69**, 42–59.
- 24 Barnes G & Gentle I (2005) *Interfacial Science: An Introduction*. Oxford University Press, Oxford.
- 25 Wüthrich K (1986) *NMR of Proteins and Nucleic Acids*. Wiley-Interscience, New York, NY.
- 26 Wishart DS & Sykes BD (1994) Chemical shifts as a tool for structure determination. *Methods Enzymol* **239**, 363–392.
- 27 Wishart DS, Bigam CG, Holm A, Hodges RS & Sykes BD (1995) ^{13}C and ^{15}N random coil NMR shifts of the common amino acids. Investigation of nearest neighbour effects. *J Biomol NMR* **5**, 67–81.
- 28 Meruka G, Dyson HJ & Wright PE (1995) 'Random coil' ^1H chemical shifts obtained as a function of temperature and TFE concentration for the peptide series GGXGG. *J Biomol NMR* **5**, 14–24.
- 29 Wong H, Bowie JH & Carver JA (1997) Solution structure and activity of caerin 1.1, an antimicrobial peptide from the Australian green tree frog, *Litoria splendida*. *Eur J Biochem* **247**, 545–555.
- 30 Zhou NE, Zhu B, Sykes BD & Hodges RS (1992) Relationship between amide proton chemical shifts and hydrogen bonding in amphipathic α -helical peptides. *J Am Chem Soc* **114**, 4320–4326.
- 31 Nilges MM & O'Donoghue SI (1998) Ambiguous NOEs and automated NOE assignment. *Proc Nucl Magn Reson Spectrosc* **32**, 107–139.
- 32 Güntert P, Berndt KD & Wüthrich K (1993) The program ASNO for computer collection of NOE upper distant constraints as input for protein structure determination. *J Biol NMR* **3**, 601–606.
- 33 Clore GM & Gronenborn AM (1991) Structures of larger proteins in solution: three- and four-dimensional heteronuclear NMR spectroscopy. *Science* **2**, 1390–1400.
- 34 Weber PL, Morrison R & Hare D (1988) Determining stereo-specific ^1H nuclear magnetic resonance assignments from distance geometry calculations. *J Mol Biol* **204**, 483–487.
- 35 Koradi R, Billeter M & Wüthrich K (1996) MOLMOL: a program for display and analysis of macromolecular structures. *J Mol Graph* **14**, 51–55.
- 36 Ramachandran GN & Sasiskharan V (1968) Conformation of polypeptides and proteins. *Adv Protein Chem* **23**, 283–437.
- 37 Timoco I (2002) Physical chemistry of nucleic acids. *Annu Rev Phys Chem* **53**, 1–15.
- 38 Middelberg APJ, He L, Dexter AF, Shen H-H, Holt SA & Thomas RK (2008) The interfacial structure and Young's modulus of peptide films having switchable mechanical properties. *J R Soc Interface* **5**, 47–54.
- 39 Adamson AW (1990) *Physical Chemistry of Surfaces*, 5th edn. Wiley, New York, NY.
- 40 Holt SA, McGillivray DJ, Poon S & White JW (2000) Protein deformation and surfactancy at an interface. *J Phys Chem B* **104**, 7431–7438.
- 41 Boncheva M & Vogel H (1997) Formation of stable polypeptide monolayers at interfaces: controlling molecular conformation and orientation. *Biophys J* **73**, 1056–1072.
- 42 Malcolm AS, Dexter AF & Middelberg APJ (2006) Foaming properties of a peptide designed to form stimuli-responsive interfacial films. *Soft Matter* **2**, 1057–1066.
- 43 Dexter AF, Malcolm AS & Middelberg APJ (2006) Reversible active switching of the mechanical properties of a peptide film at a fluid–fluid interface. *Nat Mater* **5**, 502–506.
- 44 Dexter AF & Middelberg APJ (2007) Switchable peptide surfactants with designed metal binding capacity. *J Phys Chem C* **111**, 10484–10492.
- 45 Humphrey W, Dalke A & Schulten K (1996) VMD – visual molecular dynamics. *J Mol Graph* **14**, 33–38.
- 46 Kosky P. Available at: http://minerva.union.edu/malekis/ESC24/KoskywebModules/cp_lang.htm.
- 47 Cooper S (2005) *Interfaces, Colloids and Gels*, Lecture notes. University of Durham, UK. Available at: <http://www.dur.ac.uk/sharon.cooper/lectures/colloids/interfacesweb2.html>
- 48 Chang CH & Franses E (1995) Adsorption dynamics of surfactants at the air/water interface: a critical review of mathematic models, data and mechanisms. *Colloids Surf A* **100**, 1–45.
- 49 Oron A, Davis SH & Bankov SG (1997) Long-scale evolution of thin liquid films. *Rev Mod Phys* **69**, 931–980.
- 50 Verlarde MG & Zeytounian RK (2003) *Interfacial Phenomena and the Marangoni Effect (CISM Courses and Lectures, No. 428, International Centre for Mechanical Sciences)*. Springer Verlag, Vienna.
- 51 Maeji NJ, Bray AM, Valerio RM & Wang W (1995) Larger scale multipin peptide synthesis. *Peptide Res* **8**, 33–38.

- 52 Brown AS, Holt SA, Saville PM & White JW (1997) Neutron and X-ray reflectometry – solid multilayers and crumpling films. *Aust J Phys* **50**, 391–405.
- 53 Henderson MJ, Perriman AW, Robson-Marsden H & White JW (2005) Protein–poly(silicic) acid interactions at the air/solution interface. *J Phys Chem B* **109**, 20878–20886.
- 54 Penfold J (1991) Data interpretation in specular neutron reflection. In *Neutron, X-ray and Light Scattering* (Lindner P & Zemb T, eds), pp. 223–236. Elsevier, New York, NY.
- 55 Atkinson PJ, Dickinson E, Horne DS & Richardson RM (1995) Neutron reflectivity of adsorbed beta-casein and beta-lactoglobulin at the air/water interface. *J Chem Soc Faraday Trans* **91**, 2847–2854.
- 56 Lu JR, Su TJ, Thomas RK, Penfold J & Webster J (1998) Structural conformation of lysozyme layers at the air/water interface studied by neutron reflection. *J Chem Soc Faraday Trans* **94**, 3279–3287.
- 57 Perriman AW, Henderson MJ, Holt SA & White JW (2007) Effect of the air-water interface on the stability of beta-lactoglobulin. *J Phys Chem B* **111**, 13527–13537.
- 58 Jacrot B (1976) Study of biological structures by neutron-scattering from solution. *Rep Prog Phys* **39**, 911–953.
- 59 John BK, Plant D, Webb P & Hurd RE (1992) Effective combination of gradients and crafted RF pulses for water suppression in biological samples. *J Magn Reson* **98**, 200–206.
- 60 Marion D & Wüthrich K (1983) Application of phase sensitive two-dimensional correlated spectroscopy (COSY) for measurements of ^1H – ^1H spin-spin coupling constants in proteins. *Biochem Biophys Res Commun* **113**, 967–974.
- 61 Xu RX, Word JM, Davis DG, Rink MJ, Willard DH & Gampe RT (1995) Solution structure of the human pp60c-src SH2 domain complexed with a phosphorylated tyrosine pentapeptide. *Biochemistry* **34**, 2107–2121.
- 62 Folmer RHA, Hilbers CW, Konings RNH & Nilges MM (1997) Floating stereospecific assignment revisited: application to an 18 kDa protein and comparison with J-coupling data. *J Biomol NMR* **9**, 245–258.
- 63 Engh RA & Huber R (1991) Accurate bond and angle parameters for X-ray protein-structure refinement. *Acta Crystallogr A* **47**, 392–400.

Supplementary material

The following supplementary material is available online:

Fig. S1. RQ_Z^4 versus Q_Z data and fits (solid lines) from 30 μL of a $1\text{ mg}\cdot\text{mL}^{-1}$ solution of splendipherin spread at the air/water interface at an area per molecule of 550 \AA^2 (black) and 344 \AA^2 (grey).

Fig. S2. RQ_Z^4 versus Q_Z data and fits (solid lines) from 30 μL of a $1\text{ mg}\cdot\text{mL}^{-1}$ solution of splendipherin spread at the air/water interface at an area per molecule of 275 \AA^2 (black circle) and 157 \AA^2 (grey square).

Fig. S3. RQ_Z^4 versus Q_Z data from 30 μL of a $1\text{ mg}\cdot\text{mL}^{-1}$ solution of splendipherin spread at the air/water interface at an area per molecule of 157 \AA^2 (black circle). The solid lines show the resulting fits from a one-layer model (grey) and a two-layer model (black), and the range on each axis is reduced to better show the quality of fit.

Fig. S4. CD spectra from $0.4\text{ mg}\cdot\text{mL}^{-1}$ solutions of splendipherin containing varying concentrations (v/v) of trifluoroethanol (TFE).

Fig. S5. NH to HN region of a NOESY spectrum (mixture 150 ms) of splendipherin in trifluoroethanol/water (1 : 1 v/v). NOEs between sequential NH protons are indicated.

Fig. S6. Deviation of random-coil chemical shifts of ^1H α -CH resonances of splendipherin in trifluoroethanol/water (1 : 1 v/v). A negative chemical shift difference indicates an upfield chemical shift, compared with the random-coil value.

Fig. S7. Deviation from random-coil chemical shifts of ^{13}C α -CH resonances of splendipherin in trifluoroethanol/water (1 : 1 v/v). A positive chemical shift difference indicates a downfield chemical shift compared with the random-coil value.

Table S1. Chemical shift assignments from NOESY and HSQC spectra for splendipherin.

This material is available as part of the online article from <http://www.blackwell-synergy.com>

Please note: Blackwell Publishing are not responsible for the content or functionality of any supplementary materials supplied by the authors. Any queries (other than missing material) should be directed to the corresponding author for this article.